Journal of Genetics and Genomics 46 (2019) 291–299

Contents lists available at ScienceDirect

Journal of Genetics and Genomics

Journal homepage: www.journals.elsevier.com/journal-of-genetics-and-genomics/

Original research

Nlrc3-like is required for microglia maintenance in zebrafish

Tienan Wang [a, e, 1], Bo Yan [b, e, *, 1], Liang Lou [a], Xi Lin [a], Tao Yu [a], Shuting Wu [a], Qing Lu [c], Wei Liu [d], Zhibin Huang [d], Mingjie Zhang [a], Wenqing Zhang [d, *], Zilong Wen [a, *]

[a] Division of Life Science and State Key Laboratory of Molecular Neuroscience, Center of Systems Biology and Human Health, The Hong Kong University of Science and Technology, Clearwater Bay, Kowloon, Hong Kong, China
[b] Shanghai Public Health Clinical Center, Fudan University, Shanghai, 201508, China
[c] Bio-X Institutes, Key Laboratory for the Genetics of Developmental and Neuropsychiatric Disorders, Ministry of Education, Shanghai Jiao Tong University, Shanghai, 200240, China
[d] Department of Developmental Biology, School of Basic Medical Sciences, South China University of Technology, Guangzhou, 510630, China
[e] Division of Life Science, Hong Kong University of Science and Technology, Clear Water Bay, Kowloon, Hong Kong, China

ARTICLE INFO

Article history:
Received 1 November 2018
Received in revised form
17 June 2019
Accepted 17 June 2019
Available online 22 June 2019

Keywords:
Zebrafish
Microglia
Inflammasome
NOD-like receptors

ABSTRACT

Microglia are tissue-resident macrophages residing in the central nervous system (CNS) and play critical roles in removing cellular debris and infectious agents as well as regulating neurogenesis and neuronal activities. Yet, the molecular basis underlying the establishment of microglia pool and the maintenance of their homeostasis in the CNS remain largely undefined. Here we report the identification and characterization of a mutant zebrafish, which harbors a point mutation in the nucleotide-binding oligomerization domain (NOD) like receptor gene *nlrc3-like*, resulting in the loss of microglia in a temperature sensitive manner. Temperature shift assay reveals that the late onset of *nlrc3-like* deficiency leads to excessive microglia cell death. Further analysis shows that the excessive microglia death in *nlrc3-like* deficient mutants is attributed, at least in part, to aberrant activation of canonical inflammasome pathway. Our study indicates that proper regulation of inflammasome cascade is critical for the maintenance of microglia homeostasis.

1. Introduction

Microglia are tissue-resident macrophages that reside in the central nervous system (CNS) (Barron, 1995; Hanisch and Kettenmann, 2007; Davoust et al., 2008). Recent studies have suggested that in addition to functioning as scavengers to remove cellular debris and infectious agents in the CNS, microglia are involved in many other biological processes including neurotrophic factor synthesis, synaptic pruning, and neuronal activity modulation (Trang et al., 2011; Li et al., 2012b; Nayak et al., 2014). Despite the extensive studies in the past decades, the molecular basis governing the development of microglia and their homeostasis remain largely undefined.

The NOD-like receptors (nucleotide-binding oligomerization domain like receptors, NLRs) are a class of intracellular receptors that recognize pathogen-associated molecular patterns (PAMPs) and danger-associated molecular patterns (DAMPs) (Kawai and Akira, 2009). Most of these receptors contain three function domains: an N-terminal effector domain mediating the activation of downstream signaling; a central NOD or NACHT domain (neuronal apoptosis inhibitor protein (NAIP), major histocompatibility complex class II transactivator (CIITA), incompatibility locus protein from Podospora anserina (HET-E), and telomerase-associated protein (TP1) domain) necessary for self-oligomerization; and a C-terminal leucine rich repeat (LRR) domain responsible for sensing upstream stimuli (Chen et al., 2009). Based on the type of N-terminal effector domain, NLR family is divided into 4 subfamilies, namely NLRA (A for acidic activation domain), NLRB (B for BIR – baculovirus inhibitory repeat), NLRC (C for CARD – caspase-activating and recruitment domain) and NLRP (P for PYD – pyrin domain) (Chen et al., 2009). Upon recognition of DAMPs and PAMPs, the NLR proteins oligomerize and recruit apoptosis-associated speck-like protein containing a caspase recruitment

* Corresponding authors.
E-mail addresses: bo.yan@shphc.org.cn (B. Yan), mczhangwq@scut.edu.cn (W. Zhang), zilong@ust.hk (Z. Wen).
[1] These authors contributed equally to this work.

https://doi.org/10.1016/j.jgg.2019.06.002

domain (ASC) and caspase-1 to form cytoplasmic multi-protein complexes known as inflammasomes, which leads to the activation of caspase-1, release of proinflammatory cytokines and pyroptotic cell death (Miao et al., 2011; Latz et al., 2013; Lamkanfi and Dixit, 2014). Unlike other NLR proteins, NLRP10 contains a PYD and a NACHT domain but lacks the C-terminal LRR domain (Wang et al., 2004; Damm et al., 2013), suggesting it has a distinctive role in the inflammasome activation. Indeed, both *in vitro* and *in vivo* ectopic overexpression assay has indicated that NLRP10 likely functions as a negative regulator during inflammasome activation through sequestering ASC in the cytoplasm (Wang et al., 2004; Imamura et al., 2010). Consistent with this notion, a recent study in zebrafish has shown that the inactivation of NOD-like receptor Nlrc3-like, which, like NLRP10, consists of a PYD and a NACHT but lacks the LRR domain, causes a systemic inflammatory activation of peripheral macrophages, thereby preventing peripheral macrophages from migrating into the brain (Shiau et al., 2013). However, whether Nlrc3-like is required for the maintenance of microglia is unclear.

In this study, we identified and characterized a temperature sensitive mutant zebrafish *puer*, which harbors a loss-of-function mutation in the NOD-like receptor *nlrc3-like*. When raised under the permissive temperature, *puer* mutants contained normal number of microglia but the number of microglia was drastically reduced 24 h after switched to the restricted temperature. Time-lapse imaging revealed that under the restricted temperature, *nlrc3-like* deficient microglia exhibited excessive cell death with characteristics similar to that of pyroptosis, including cell swelling, plasma-membrane rupture and pro-inflammatory cytokine production. The microglia cell death in *nlrc3-like* deficient mutants could be partially rescued by the suppression of Asc function, a key regulator of inflammasome cascade.

2. Results

2.1. Microglia defect in puer mutants is temperature sensitive

To uncover new regulators in microglia development, we conducted an N-ethyl-N-nitrosourea (ENU) based forward genetic screening in zebrafish. By using Neutral Red (NR) staining of microglia (Herbomel et al., 2001), we identified a mutant line *puer* (puer represents a kind of Chinese tea) (*nlrc3*^{hkz6} allele), in which the NR staining signal in the brains of the homozygous embryos was reduced at 3 days post-fertilization (dpf). We noticed that the degree of the reduction of NR signal varied among the mutant embryos in the same clutch offspring under normal breeding condition (28.5 °C), suggesting that *puer* could be a temperature sensitive mutant. To test this hypothesis, we raised the mutants at different temperatures and stained with NR after they reached the developmental stage equivalent to 3 dpf. Indeed, *puer* mutants were devoid of NR signal under the restricted temperature at 34 °C, but harbored decent number of NR-positive cells under the permissive temperature at 24 °C (Fig. 1A). The lack of NR staining under the restricted temperature in *puer* mutants was likely due to the loss of microglia because the expression of apolipoprotein Eb (*apoeb*), a well-known microglia marker in zebrafish (Herbomel et al., 2001), was hardly detectable in *puer* mutants (Fig. 1B). In line with the lack of microglia phenotype, a pronounced accumulation of un-engulfed apoptotic neurons (with weak acridine orange (AO) staining signal) was observed in the brains of *puer* mutants under the restricted temperature (Fig. S1A). Notably, the *puer* mutation appeared to have little effect on general development of macrophages as shown by the normal expression of macrophage-specific marker *mfap4* (Zakrzewska et al., 2010) at 1 dpf under the restricted temperature (Fig. 1C), but did cause

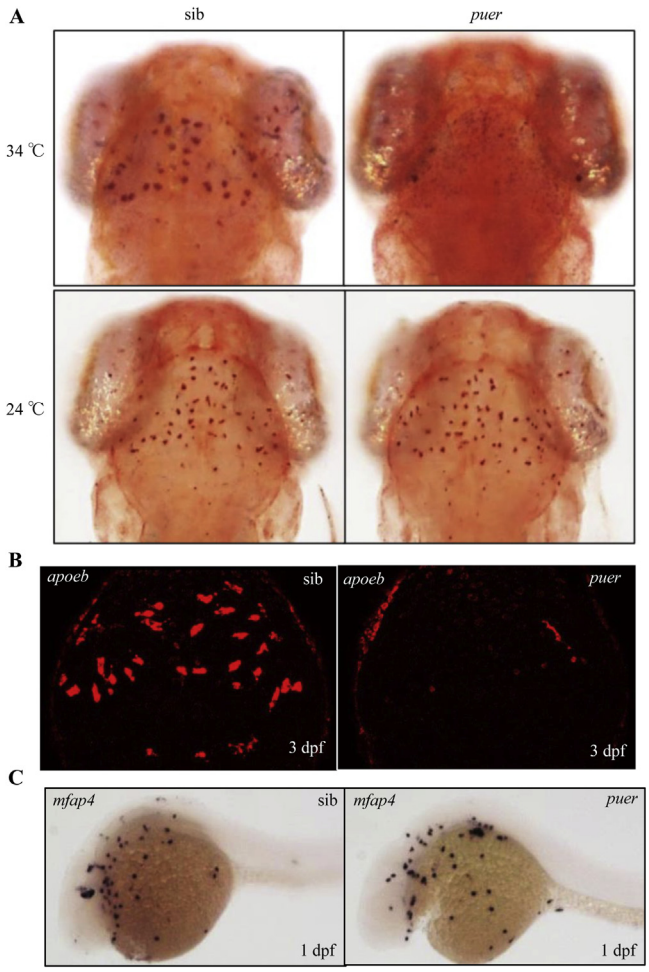

Fig. 1. Microglia defect in *puer* mutants is temperature sensitive. **A**: NR staining indicates that microglia in the brain of 3 dpf *puer* mutant are significantly reduced under the restricted temperature (34 °C) (upper) but remain comparable to that of siblings under the permissive temperature (24 °C) (below). **B**: *apoeb* WISH shows lack of microglia in the brains of 3 dpf *puer* mutants under the restricted temperature. **C**: *mfap4* WISH indicates normal development of peripheral macrophages in 1 dpf *puer* mutant embryos.

abnormal inflammation as indicated by the formation of inflammatory clusters composed of macrophages and neutrophils in the trunk and tail regions at later stages (Fig. S1B).

2.2. The puer mutant gene encodes Nlrc3-like protein

To unveil the genetic lesion underlying *puer* mutant phenotype, positional cloning was carried out. Bulk segregation analysis mapped the *puer* mutation to chromosome 15 (Fig. S2A) and fine mapping further positioned the mutation to a 40 kb region containing three candidate genes, *chordc1a* (cysteine and histidine-rich domain containing 1a), *nlrc3-like*, and *numa1* (nuclear mitotic apparatus protein 1). DNA sequencing analysis identified a T to A single mutation in the exon 6 of *nlrc3-like* gene, resulting in the substitution of the amino acid isoleucine (I) 495 by asparagine (N) (Fig. S2B). Because no mutation was found in other two candidate genes, we suspected that *puer* mutant phenotype was caused by this T to A mutation in *nlrc3-like* gene. Indeed, ectopic expressing WT (wild-type) but not I_{495}—N mutant Nlrc3-like in *puer* mutants could partially rescue the microglia phenotype (Fig. 2A), confirming that *nlrc3-like* is the corresponding gene for *puer* mutant phenotype. This I_{495}—N mutation appeared to be a recessive mutation

because *puer* heterozygous embryos did not exhibit any detectable microglia phenotype (data not shown).

To understand the molecular basis underlying the I_{495}—N mutation in Nlrc3-like protein, we constructed a 3D structural model of Nlrc3-like and compared to mammalian NLRC4, one of the NLRP members with the known 3D structure (Hu et al., 2013). Result showed that the two proteins were highly similar in primary sequences and 3D structure, especially in the NACHT domain where the mutation occurs in *puer* mutants (Fig. 2B and C). Similar to that of NLRC4, the NACHT domain of Nlrc3-like proteins contains 4 subdomains: NBD (nucleotide-binding domain), HD1 (helical domain 1), WHD (winged-helix domain), and HD2 (helical domain 2). The NBD forms a three-layered α/β structure (Fig. 2B and C), and notably, the I_{495}—N mutation is located at α6 (Fig. 2B and C, marked in red), a region corresponding to human NLRC4 α8, which is essential for the maintenance of monomeric conformation of NLRC4 proteins (Erzberger and Berger, 2006; Danot et al., 2009; Hu et al., 2013; Diebolder et al., 2015; Zhang et al., 2015). We therefore speculated that the I_{495}—N mutation might cause a self-oligomerization or aggregation, resulting in the disruption of

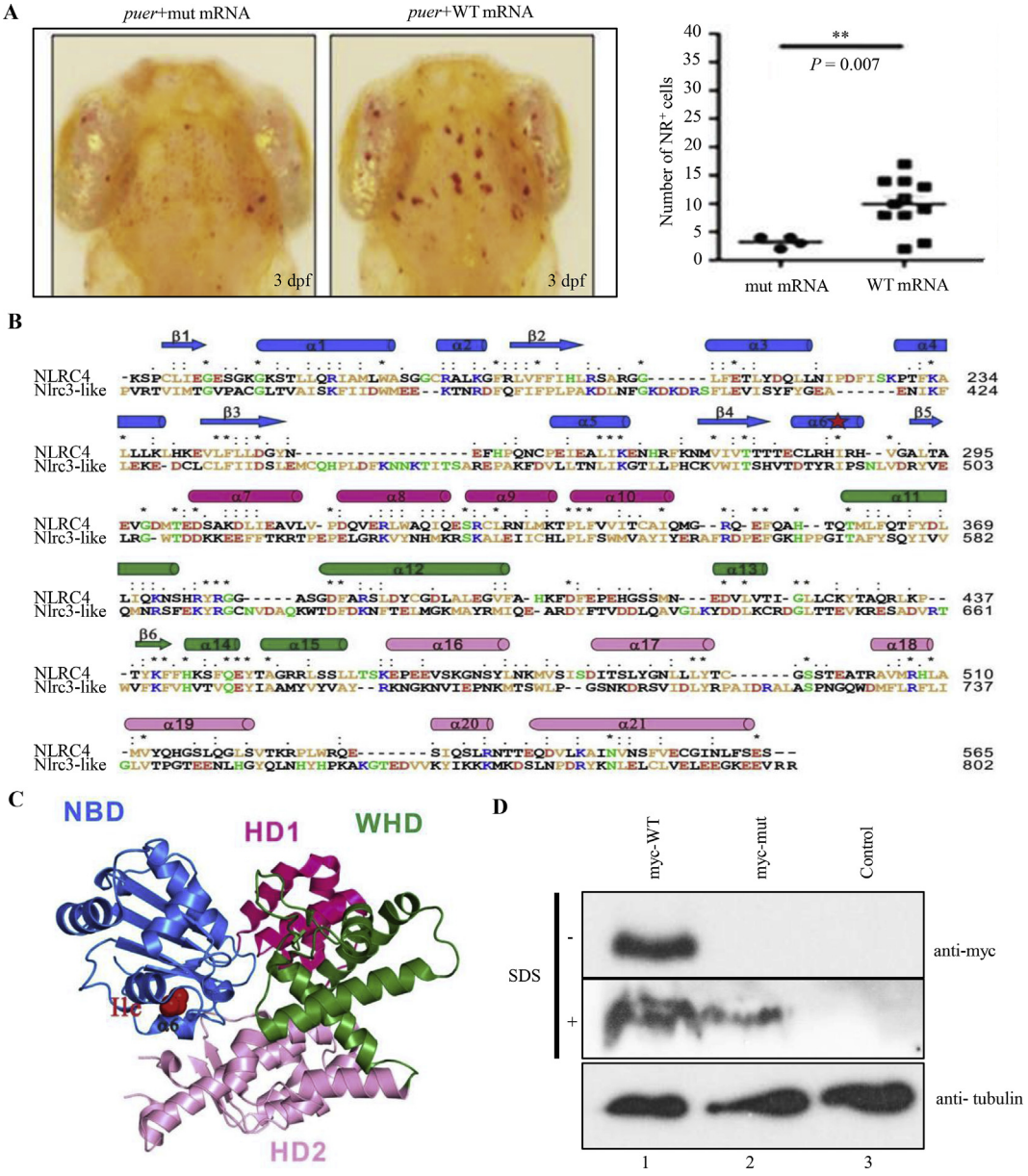

Fig. 2. The *puer* mutant gene encodes Nlrc3-like with an aggregation promoting mutation in the NACHT domain. **A**: NR staining (left panels) shows that injection of *in vitro* synthesized WT but not mutant *nlrc3-like* mRNA into *puer* mutant embryos can partially rescue the microglia defect. The right panel is quantification assay and each dot represents one embryo. **B**: Protein sequence alignment of the NOD module of human NLRC4 and zebrafish Nlrc3-like. NBD (nucleotide-binding domain) is colored in blue, HD1 (helical domain 1) in magenta, WHD (winged-helix domain) in green, and HD2 (helical domain 2) in pink. The mutation site I_{495} is highlighted by a red pentagram in α6. Residues are colored according to their hydrophobicity (yellow for hydrophobic residues, blue for positively charged residues, red for negatively charged residues and green for other polar residues). Residues conservation is labeled above the sequence: star for absolutely identical, dots as highly similar. **C**: Ribbon-diagram representation of NOD module of Nlrc3-like. Domain labeling is colored as in **B**. The position of the conserved I_{495} is indicated by the red sphere in α6. **D**: Western blotting shows that the mutant Nlrc3-like protein is detected in the presence (middle panel) of SDS but not detected in the absence (upper panel) of SDS. Lanes 1 and 2 represent myc-tagged WT and myc-tagged mutant Nlrc3-like, respectively. The bottom panel is β-tubulin control.

Nlrc3-like function. To test this possibility, we expressed myc-tagged WT and mutant Nlrc3-like by injecting *in vitro* synthesized mRNA into fertilized WT embryos. 9 h post-injection, protein extracts were prepared with lysis buffer without sodium dodecyl sulfate (SDS) and subjected to polyacrylamide gel electrophoresis in the presence and absence of SDS. Western blotting showed that the mutant proteins were detected only in the presence of SDS, while WT proteins could be detected in both conditions (Fig. 2D). These data strongly suggest that the Nlrc3-like mutant proteins form large aggregated complexes which failed to enter the polyacrylamide gel or transfer to polyvinylidene fluoride membrane in the absence of SDS. Based on these observations, we conclude that the I_{495} to N mutation causes self-aggregation of Nlrc3-like proteins, which in turn diminishes its restraint on Asc and results in the activation of inflammasome pathway. As the kinetics of protein folding is sensitive to temperatures, the aggregation property of the mutant Nlrc3-like proteins explains, at least in part, the temperature sensitive microglia phenotype of *puer* mutants.

2.3. Microglia undergo excessive cell death in puer mutants

A previous study by Shiau et al. has indicated that the loss of Nlrc3-like function in zebrafish leads to activation and aggregation of peripheral macrophages, thereby preventing them from migrating into the brain (Shiau et al., 2013). However, the role of Nlrc3-like in microglia development after colonization in the brain remains undefined. To address this issue, we raised the mutant embryos under the permissive temperature (24 °C) for 5 days to allow microglia to colonize in the brains (Fig. 3A). The mutant embryos were then placed at the restricted temperature (34 °C) for 12−24 h and stained with NR. Results showed that the number of recovered microglia was significantly reduced after 12 h incubation at 34 °C and very few microglia remained in the mutant brains after 24 h (Fig. 3A and B). Two possible mechanisms, *in situ* cell death of microglia and egression of microglia, could account for the disappearance of microglia after temperature shift. To distinguish these two possibilities, we performed time-lapse imaging on *puer* mutants in *Tg(coro1a:eGFP;lyz:Dsred2)* or *Tg(coro1a:DsRedx;lyz:eGFP)* transgenic background, in which macrophages (including microglia) and neutrophils were marked by distinct colors. It was shown that the mutant microglia vanished locally inside the brain and microglia egression was never observed (Fig. 3C–G; Movie S1). These data indicate that the reduction of microglia in *puer* mutants under the restricted temperature is largely attributed to cell death. Intriguingly, severe inflammation was induced by microglia cell death as indicated by the infiltration of neutrophils surrounding the dying microglia (Fig. 3C–G; Movie S1). Given the fact that NLRs-mediated inflammasome activation is known to induce pyroptosis (Bergsbaken et al., 2009; Miao et al., 2011; Aachoui et al., 2013; Jorgensen and Miao, 2015), these data suggest that the loss of microglia in *puer* mutants under the restricted temperature could be caused by excessive pyroptosis.

Supplementary data related to this article can be found at https://doi.org/10.1016/j.jgg.2019.06.002.

To support this hypothesis, we performed time-lapse imaging with a higher magnification optic lens coupled with differential interference contrast (DIC) filter to monitor the dynamic behaviors of microglia in *puer* mutants and siblings. In the control siblings, majority of microglia exhibited a ramified morphology and extended their protrusions constantly for phagocytosis (Fig. 3H–L) (Svahn et al., 2013). Occasionally, they contacted each other but separated shortly after (Fig. 3I–L). In contrast, upon switched to the restricted temperature, the mutant microglia displayed a round-shaped morphology with swelling cytoplasm (Fig. 3M). Strikingly, many mutant microglia formed a balloon-shaped cytoplasm structure and subsequently budded out of the cell membrane (Fig. 3M–Q; Movie S2). Finally, these pre-mortal microglia ruptured their membrane (Fig. 3R–V), lost DsRed-positive cytoplasm fluid and condensed into cellular debris (Fig. 3T and U, black arrows). Notably, a substantial portion of the mutant microglia fused together or phagocytosed each other to form one large cell before they died (Fig. S3), presumably due to the activation and inflammatory response of these cells. These dynamic changes of microglia morphology and the induction of inflammatory response resemble the characteristic of pyroptosis reported previously (Watson et al., 2000; Sun et al., 2005; Fernandes-Alnemri et al., 2007; Breitbach et al., 2009; Miao et al., 2011). To support this idea, we knocked down the expression of *gsdmea* or *gsdmeb*, the two zebrafish counterparts of mammalian gasdermin family genes known to be essential for pyroptosis (Kayagaki et al., 2015; Shi et al., 2015; Kovacs and Miao, 2017; Wang et al., 2017) in *puer* mutants by morpholino oligonucleotides (MO). Results showed that *gsdmea* but not *gsdmeb* knockdown could partially rescue microglia cell death in *peur* mutants (Figs. 3W and S4A–D), indicating that the microglia in *puer* mutants indeed undergo pyroptosis upon switched to the restricted temperature. Interestingly, the death of microglia was independent of neutrophil infiltration as the depletion of neutrophils in *puer* mutants by *runx1* MO (Jin et al., 2012) had little effect on the death of microglia (Fig. S5A and B).

Supplementary data related to this article can be found at https://doi.org/10.1016/j.jgg.2019.06.002.

2.4. Microglia cell death in puer mutants is partially triggered by aberrant activation of inflammasome pathway

It has been shown that mammalian NLRP10 predominatly functions as a negative regulator to suppress inflammasome pathway by sequestering ASC (Wang et al., 2004; Imamura et al., 2010). Given the fact that zebrafish Nlrc3-like has a structure similar to mammalian NLRP10 (Fig. S2C), we therefore deduce that Nlrc3-like may act as a negative regulator and the loss of Nlrc3-like function eventually leads to hyper-activation of inflammasome pathway, resulting in microglia cell death. To support this hypothesis, we generated an *asc*-deficient fish, $asc^{\Delta 31}$, in which a 31 bp coding sequence was deleted, leading to the generation of a truncated Asc protein lacking the entire CARD domain and a small part of PYD domain (Fig. S6A–C). The *asc*-deficient fish were outcrossed with *puer* mutants and the resulting *puer;*$asc^{\Delta 31}$ double mutants were used to test whether the suppression of inflammasome pathway activation could reduce microglia cell death. Indeed, microglia number was partially recovered in *puer;*$asc^{\Delta 31}$ double mutants, suggesting that aberrant hyper-activation of inflammasome pathway contributes to the death of microglia in *puer* mutants (Fig. 4A and B). To further support this notion, we examined the expression of interleukin 1β (*il1β*), a pro-inflammatory cytokine known to be induced upon inflammasome activation (Kayagaki et al., 2011; Gurung et al., 2012; Lamkanfi and Dixit, 2014). Result showed a robust *il1β* expression in the mutant microglia under the restricted temperature but not in WT microglia (Fig. 4C). Consistent with this result, the mRNA levels of several inflammasome activation related/pro-inflammatory cytokines were also elevated in *puer* mutants (Fig. 4D). Taken together, these data demonstrate that the microglia cell death in *puer* mutants is caused, at least in part, by the aberrant activation of inflammasome pathway.

2.5. The microglia cell death in puer mutants is cell-autonomous

Since *nlrc3-like* was highly expressed in a variety of tissues (Fig. S7), we next sought to determine whether the death of microglia in *puer* mutants was cell-autonomous or non-cell-

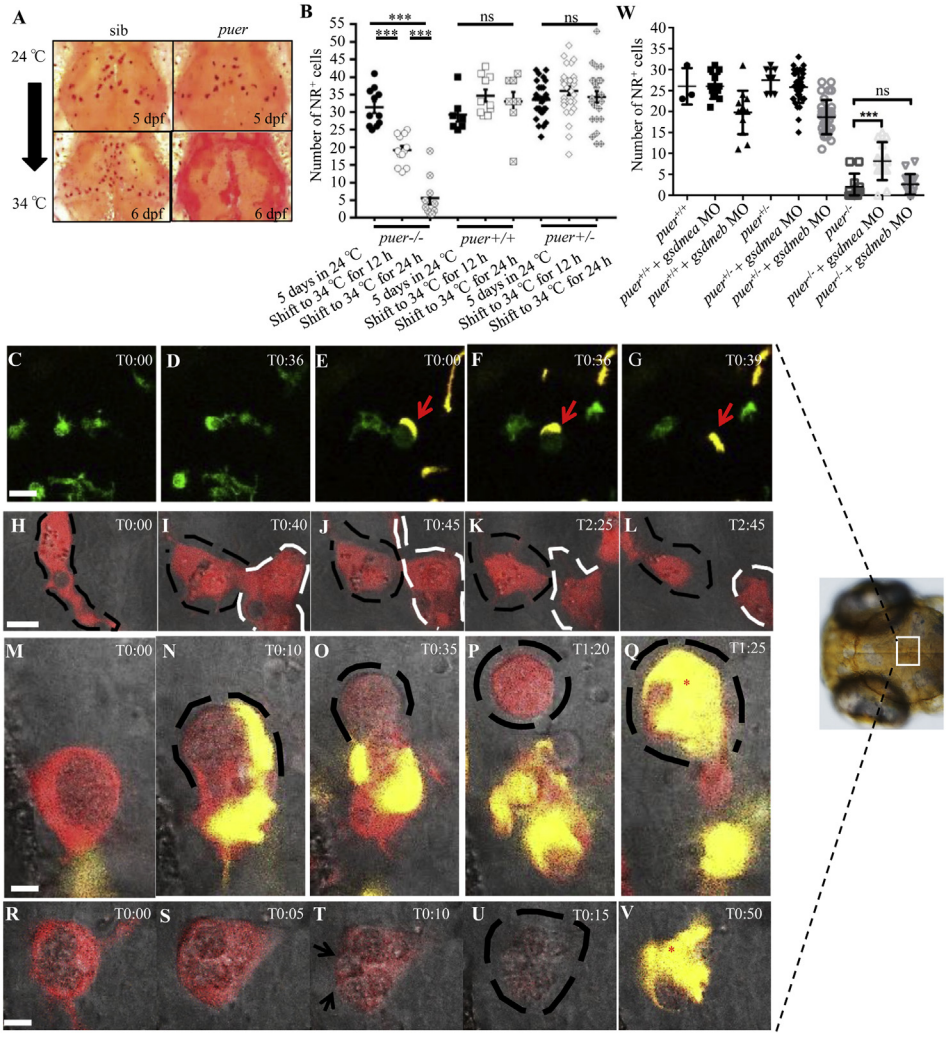

Fig. 3. Microglia in *puer* mutants undergo excessive cell death. **A**: NR staining indicates that microglia colonize the *puer* mutant brains normally under permissive temperature (upper panels), but these recovered mutant microglia disappear 24 h post-switching to the restricted temperature (lower panels). **B**: Quantification of microglia number in *puer* mutants before and after switching to the restricted temperature for 12 h and 24 h. Microglia are scored by NR staining and each dot represents one embryo. **C–G**: Time-lapse imaging (20 × objective) of *Tg(coro1a:eGFP;lyz:DsRed2)* shows normal behavior of microglia in the brains of siblings (**C** and **D**) and the disappearance of microglia and infiltration of neutrophils in the *puer* mutant brains (**E**–**G**). Microglia and neutrophil are labeled in green and yellow, respectively. T represents time frame of imaging (hour and minute). Scale bar, 20 μm. **H–L**: Time-lapse imaging (40 × objective coupled with 2.5 times zoom-in) of *Tg(coro1a:DsRedx;lyz:eGFP)* reveals normal morphological change and dynamic behavior of microglia (red) in WT embryos. T represents time frame of imaging (hour and minute). Scale bar, 10 μm. **M–V**: Time-lapse imaging (40 × objective coupled with 2.5 times zoom-in) of *Tg(coro1a:DsRedx;lyz:eGFP)* indicates that mutant microglia (more than 50% during 24 h imaging) undergo a typical morphological changes of pyroptosis including cell body swelling, cytoplasm membrane rupture, and diluted cytoplasm content (**R**–**U**), accompanied with neutrophil infiltration (**V**). A substantial number of pyroptotic microglia form a balloon-shaped cytoplasm structure (indicated by asterisk) and bud out of the cytoplasm membrane (**M–Q**). Microglia and neutrophil are labeled by red and yellow fluorescence, respectively. T represents time frame of imaging (hour and minute). Scale bar, 5 μm. **W**: Quantification of microglia number in the *puer* mutants and siblings injected with control MO, *gsdmea* MO or *gsdmeb* MO. The injected embryos were incubated under the restricted temperature for 3 days and then stained with NR. Each dot represents one embryo. ns, no significance. ***, $P < 0.001$.

autonomous. To address this question, we generated a transgenic line *Tg(coro1a:nlrc3-like)*, in which the expression of WT *nlrc3-like* was under the control of leukocyte-specific *coro1a* promoter (Fig. S7) (Li et al., 2012a). The *Tg(coro1a:nlrc3-like)* fish were outcrossed with *puer* mutants and the resulting *Tg(coro1a:nlrc3-like);puer* transgenic mutant fish were collected for temperature shift assay. In *Tg(coro1a:nlrc3-like);puer* transgenic mutants, the microglia number was comparable to that in WT and the neutrophil infiltration of the brains in *puer* mutants was also completely abolished (Fig. 5A and B). These results show that over-expression of WT *nlrc3-like* in myeloid cells is sufficient to rescue the microglia phenotype, indicating that Nlrc3-like acts cell-autonomously to maintain the homeostasis of microglia.

3. Discussion

Here, we report the identification and characterization of a zebrafish mutant *puer*, which harbors a point mutation (I to N change at the position of amino acid 495) in the Nlrc3-like, resulting in microglia cell death in a temperature sensitive manner. We further show that loss of Nlrc3-like function results in aberrant activation of inflammasome pathway in an Asc-dependent manner. Interestingly, similar to human NLRP10 (Wang et al., 2004; Damm et al., 2013; Shiau et al., 2013), zebrafish Nlrc3-like consists of a PYD and a NACHT domain but lacks the LRR domain at the C-terminus, suggesting that Nlrc3-like may play a role similar to human NLRP10. This argument is supported by previous findings showing

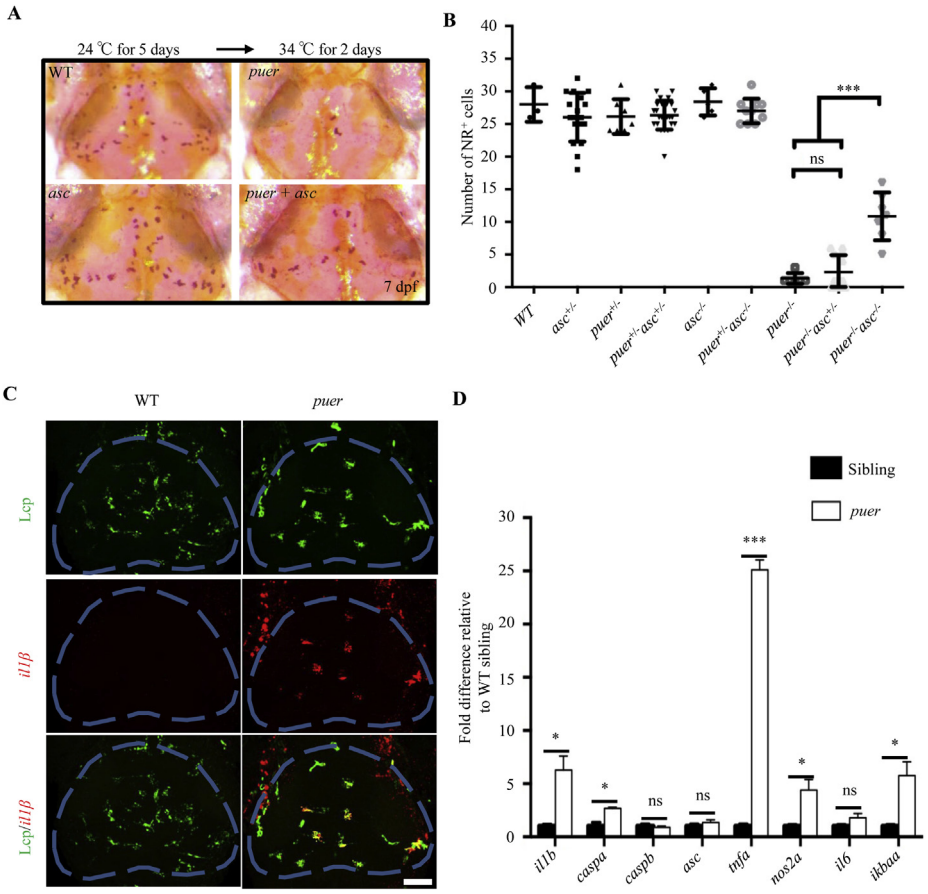

Fig. 4. Aberrant activation of inflammasome pathway contributes to microglia cell death in *puer* mutants. **A**: NR staining of WT, *puer*, $asc^{\Delta 31}$ and *puer*;$asc^{\Delta 31}$ embryos shows that the inactivation of Asc function partially rescues microglia defect in *puer* mutants. **B**: Quantification of microglia (NR^+ cells) number in siblings, *puer* and $asc^{\Delta 31}$ single mutants and *puer*;$asc^{\Delta 31}$ double mutants. Embryos were incubated at 24 °C for 5 days and shifted to 34 °C for 2 days. Each dot represents one embryo. n.s., no significance. ***, $P < 0.001$. **C:** *il1β* WISH (red) and anti-Lcp1 antibody (green) co-staining reveals a robust increase of *il1β* expression in *puer* mutant microglia (right panels) compared to WT microglia (left panels). Scale bar, 50 μm. **D**: mRNA expression levels of inflammasome activation related pro-inflammatory cytokines in the brain region of *puer* mutants and siblings. Embryos were incubate at 34 °C for 3 days and *puer* mutants and siblings were identified based on accumulation of apoptotic neuron body in the brain. Embryos were then shifted to 24 °C for 1 day and subsequently shifted to 34 °C for 12 h before the brain tissue was dissected. mRNA was collected from three independent biological replicates. ns, no significant difference. *, $P < 0.05$; ***, $P < 0.001$.

that overexpressing human NLRP10 in cell lines and in mice inhibits inflammasome pathway activation by sequestering ASC (Wang et al., 2004; Imamura et al., 2010). Thus, both zebrafish Nlrc3-like and human NLRP10 act as negative regulator of inflammasome pathway. Intriguingly, mouse NLRP10 does not seem to function in a similar fashion since ectopically overexpressing mouse NLRP10 in mice does not inhibit inflammasome pathway activation (Imamura et al., 2010; Damm et al., 2013). It will be interesting to investigate the molecular basis underlying the different functions of zebrafish Nlrc3-like, mouse NLRP10 and human NLRP10.

Our study has shown that the dynamic behaviors of dying microglia in *puer* mutants recapitulate the characteristics of pyroptosis described previously in cell lines (Watson et al., 2000; Sun et al., 2005; Fernandes-Alnemri et al., 2007; Breitbach et al., 2009). Interestingly, *gsdmea* MO could partially rescue microglia cell death in *puer* mutants, whereas *gsdmeb* MO has no obvious effect. This result indicated that zebrafish *gsdmea* is the functional homolog of mammalian *GASDERMIN D* in pyroptosis pathway. The partial rescue by *gsdmea* MO could be due to incomplete inactivation of Gsdmea function or existence of a pyroptosis-independent microglia cell death. Further investigation is required to clarify this issue.

Interestingly, the inactivation of *asc* only partially rescues the microglia cell death in *puer* mutants. Given the fact that the entire CARD domain and a small part of PYD domain are presumably deleted in $asc^{\Delta 31}$ fish, we speculate that the partial rescue in $asc^{\Delta 31}$;*puer* double mutants suggests the existence of an Asc-independent microglia cell death. This argument is supported by recent studies showing that two distinct pathways, canonical and non-canonical inflammasome pathways can trigger pyroptosis (Kayagaki et al., 2011, 2015; Man and Kanneganti, 2015). In the canonical pathway, ASC is required for caspase-1 processing and GASDERMIN D cleavage, whereas an ASC-independent capase-4, 5 and 11 activations are involved in the non-canonical pathway. It will be of interest to investigate whether this Asc-independent microglia cell death in *puer* mutants is caused by a non-canonical inflammasomes pathway-mediated pyroptosis or by a completely different type of cell death.

Another interesting observation is that, while mutant microglia undergo rapid cell death upon switching to the restricted temperature, peripheral macrophages do not exhibit extensive cell death. Instead, peripheral macrophages and neutrophils in *puer* mutants form inflammatory clusters in the trunk and tail regions (Fig. S1B). The distinct outcome of microglia and peripheral macrophages in *puer* mutants could be attributed to the intrinsic differences of these two cell types or the extrinsic distinctness in the micro-environments where they reside. We favor the latter possibility

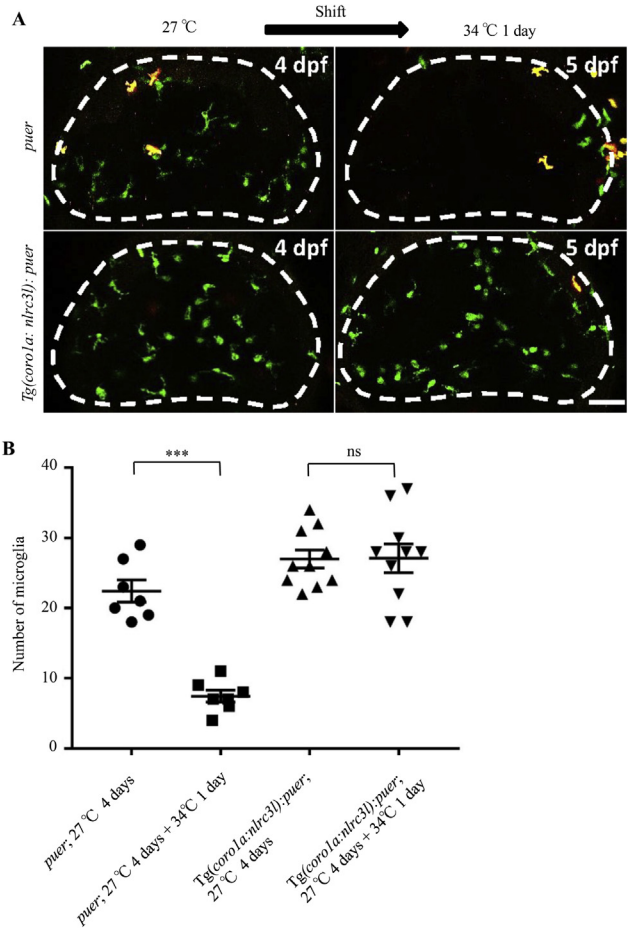

Fig. 5. Nlrc3-like acts cell-autonomously. **A**: Fluorescent images of the brains of *puer;Tg(coro1a:eGFP;lyz:DsRed2)* mutants (upper panels) and *Tg(coro1a:nlrc3-like);puer;Tg(coro1a:eGFP;lyz:DsRed2)* rescue fish (lower panels) expressing WT *nlrc3-like* in leukocytes using *coro1a* promoter. Microglia are labeled by GFP and dash lines indicate the midbrain region. Embryos were raised at 27 °C (left panels) for 4 days and then switched to 34 °C (right panels) for 24 h. Scale bar, 50 μm. **B**: Quantification of microglia number in *puer;Tg(coro1a:eGFP;lyz:DsRed2)* mutants and *Tg(coro1a:nlrc3-like);puer;Tg(coro1a:eGFP;lyz:DsRed2)* rescue fish expressing WT *nlrc3-like* in leukocytes. Embryos were raised at 27 °C for 4 days and then switched to 34 °C for 24 h. Each dot represents one embryo. ***, $P < 0.001$.

because microglia in the brain are known to actively engulf apoptotic neurons (Herbomel et al., 2001; Peri and Nusslein-Volhard, 2008; Latz et al., 2013), which could activate inflammasome cascades, resulting in excessive death of microglia. This hypothesis can be tested by generating phagocytosis-deficient mutants by targeting key factors essential for phagocytosis (Grimsley et al., 2004; Park et al., 2007; Fricker et al., 2012).

In sum, our findings reveal that aberrant activation of canonical inflammasome cascades leads to excessive microglia cell death, indicating that the regulation of inflammasome pathway is essential for the maintenance of microglia homeostasis.

4. Materials and methods

4.1. Fish lines

AB, WIK, *puer* (*nlcr3l*^{hkz6} allele), *asc*$^{\Delta 31}$(*asc*^{hkz7}), *Tg(coro1a:eGFP;lyz:DsRed2)hkz05t; nz50t* (Hall et al., 2007; Li et al., 2012a), *Tg(coro1a:DsRedx;lyz:eGFP)hkz011t;nz117t* (Hall et al., 2007; Xu et al., 2016), *Tg(coro1a:nlrc3-like)hkz22*Tg and *Tg(mpeg1:loxP-DsRedx-loxP-GFP) hkz015t* (Xu et al., 2016) strains were used in this study.

4.2. ENU mutagenesis and NR staining

ENU (Sigma, USA) mutagenesis was carried out as described (Mullins et al., 1994; Solnica-Krezel et al., 1994). NR staining was performed as reported (Herbomel et al., 2001).

4.3. Genetic mapping

Bulk segregant analysis mapped the *puer* mutant lesion to chromosome 15 flanked by two SSLP markers z13230 and z6024. High-resolution mapping further narrowed down the mutation in a 600–700 kb physical distance flanked by SSLP markers z9773 and A3. Sequencing the coding regions of candidate genes revealed a T to A mutation in *nlrc3-like*, resulting in a substitution of amino acid I_{495} with N. The *puer* mutants were genotyped by PCR of genomic DNA followed by *Tfi*I restriction digestion. The primers (*peur*-F and *puer*-R) used for genotyping are listed in Table S1.

4.4. Plasmids and in vitro RNA synthesis

Full length coding sequence (CDS) of WT and mutant *nlrc3-like* (ENSDART00000186320.1) obtained from 3 dpf WT and *puer* mutants were subcloned into pCS2$^+$ vector with 5 × myc tag at the N-terminus to generate *pCS2*$^+$*-5×myc-nlrc3l-wt* and *pCS2*$^+$*-5×myc-nlrc3l-mt* constructs. The myc-tagged *nlrc3-like* mRNA was synthesized *in vitro* by using SP6 polymerase with linearized *pCS2*$^+$*-5×myc-nlrc3l-wt* and *pCS2*$^+$*-5×myc-nlrc3l-mt* DNA. Transgenic construct *pTAL-coro1a-nlrc3l* was generated by inserting full-length WT *nlrc3-like* CDS into *pTAL-coro1a-SV40* vector derived from *pTAL-coro1a-eGFP-SV40* (Li et al., 2012a).

4.5. Protein extraction and Western blotting

In vitro synthesized myc-tagged WT or mutant *nlrc3-like* mRNA was injected into one-cell stage of WT zebrafish embryos. 9 h post-injection, whole protein lysate was prepared from injected embryos with protein lysis buffer (50 mM Tris, 100 mM NaCl, 1% NP40, 2 mM EDTA, 2 mM EGTA, 5% glycerol, 10 mM NaF, 2 μg/mL aprotinin, 20 mM β-glycerolphosphate, 1 mM DTT, 1 μM leupeptin, 1 μM pepstatin, 1 mM PMSF, 20 mM PNPP, and 50 μM sodium vanadate) with and without SDS. Equal amount of protein lysate was mixed with loading sample buffer (2 mM β-mercaptoethonal, 4% glycerol, 0.04 M Tris-HCl, pH6.8, 0.01% bromophenolblue) with and without SDS (2%) and subjected to polyacrylamide gel electrophoresis (8%) in the presence and absence of SDS (10%), respectively. The proteins were then transferred to PVDF membrane via wet electroblotting. Goat anti-myc (ab9132, Abcam, UK)/mouse anit-β-Tubulin (sc-23949, Santa Cruz, USA) antibody were used as the primary antibody and horseradish peroxidase-conjugated donkey anti-goat lgG (Abcam ab97110)/goat anti-mouse (31430, Thermo Fisher Scientific, USA) was used as the secondary antibody.

4.6. Time-lapse imaging

Time-lapse imaging with low magnification (20 ×) was performed as previously reported with some modifications (Zhen et al., 2013). 3 dpf zebrafish embryos raised at 24 °C were mounted in 1% low-melting agarose containing 0.01% tricaine and covered by 0.01% tricaine containing embryo water and subjected to time-lapse imaging using Leica SP8 confocal microscope at 34 °C for 24 h. High-magnification (40 × water objective coupled with water immersion micro dispenser) imaging was carried out the same as low magnification imaging except that zebrafish embryos were mounted in 0.8% low melting agarose without tricaine and covered by embryo water without tricaine. Imaging was taken with

3 min and 5 min interval for low and high magnification imaging, respectively. The z-stack was set as total 120–150 μm with 3 μm step size for embryonic brain.

4.7. MO injection

2 nL mixture of *runx1* MO-1 (5′-TGTTAAACTCACGTCGTGGCTCTC-3′) and *runx1* MO-2 (5′-AATGTGTAAACTCACAGTGTAAAGC-3′) at final concentration of 0.6 mM and 1 mM respectively was injected into embryos at one-cell stage as previously reported (Jin et al., 2009). *gsdmea sp* MO (5′- TCATAGTGTTTCCTAACCTTCCTCT-3′), *gsdmeb* ATG MO (5′- TGCAAACATCTTCAATGCTGACAAG-3′) and standard control MO were designed and synthesized by Gene Tools (USA). 1.5 nL *gsdmea sp* MO (0.5 mM) or *gsdmeb* ATG MO (1 mM) or control MO (0.5 mM) was injected for each embryo.

4.8. DsRed reporter assay

The protocol was described as previous reported (Li et al., 2011). Briefly, *pCS2-gsdmeb-ATG-DsRedx* reporter construct was generated by replacement of 5′ region of DsRedx coding sequence with *gsdmeb* MO target sequence. The newly generated construct was injected into embryos at one-cell stage with or without MO. The DsRedx signals in the embryos were observed at 1.5 dpf.

4.9. Whole mount in situ hybridization (WISH) and antibody staining

Antisense DIG labeled RNA probes for *apoeb* (ENSDART00000058965.6, from nucleotides −6 to +1321 of cDNA) (Herbomel et al., 2001), *il1b* (BC098597, full-length CDS) (Yan et al., 2014), and *nlrc3-like* (ENSDART00000186320.1, full-length CDS) were synthesized *in vitro* and WISH was carried out according to standard protocol (Westerfield, 1995). To examine the co-expression of Lcp and *il1b*/*nlrc3-like*, Lcp antibody staining was performed after *il1b* or *nlrc3-like* fluorescent *in situ*. For *il1b* or *nlrc3-like* fluorescent *in situ*, embryos were first hybridized with Dig-labeled RNA probe as previous described. After washed and blocked, embryos were incubated with peroxidase (POD)-conjugated anti-flu antibody (1:500) (Roche, Mannheim, Germany) and detected with AF 555 tyramide substrate (Molecular Probes, USA). After fluorescent *in situ*, anti-Lcp (Jin et al., 2009) was performed and visualized by AF488 donkey anti-rabbit (1:400) (Thermo Fisher Scientific) (Jin et al., 2009; Zhen et al., 2013).

4.10. Neutral red (NR) staining

Embryos were incubated in NR staining solution (N6264, Neutral Red solution (0.5%), Sigma, 1:1000 in PTU egg water) for ~5 h at 28.5 °C.

4.11. Sudan black (SB) staining

Embryos were fixed in 4% PFA for 2 h at room temperature and then washed with PBST for 4 × 5 min. The embryos were then incubated in SB for 25 min at room temperature and washed out by 70% ethanol 5 × 30 min.

4.12. Acridine orange (AO) staining

Zebrafish embryos were incubated in AO solution (5 μg/mL) for 0.5–1 h and washed with egg water before imaging (Peri and Nusslein-Volhard, 2008).

4.13. RNA extraction and semi-quantitative/quantitative RT-PCR

The brain tissues were collected to RLT buffer on ice, and the RNA extraction was performed using QIAGEN RNeasy Mini Kit (German). cDNA was prepared by using Invitrogen SuperScript™ II Reverse Transcriptase kit (USA). Semi-quantitative PCR was performed as described previously described (Yan et al., 2014). Quantitative RT-PCR was performed with SYBR Green Supermix (Promega, USA). The primers used for RT-PCR are listed in Table S1.

4.14. Generation of $asc^{\Delta 31}$ mutants by CRISPR/Cas9

asc (ENSDARG00000040076) gRNA (5′-ACGCGGTTTCTGTAA-CAG-3′) was designed based on the website http://crispr.mit.edu/ (Ran et al., 2013) and *Cas9* mRNA was synthesized *in vitro* as reported (Imamura et al., 2010; Chang et al., 2013; Damm et al., 2013). The gRNA and *Cas9* mRNA were co-injected into the one-cell stage embryos and the founders with germline transmission were identified by PCR. The primers (*asc*-F and *asc*-R) used for PCR genotyping are listed in Table S1.

4.15. Statistical analysis

Two-tailed Student's *t*-test was applied for statistical analysis. If $P < 0.05$, results were considered to be significant. Values were plotted as mean ± s.e.m.

Acknowledgments

This work was supported by the National Natural Science Foundation of China (81801977, 31761163008), Shanghai Sailing Program (18YF1420400), the Outstanding Youth Training Program of Shanghai Municipal Health Commission (2018YQ54), the Research Grants Council of the HKSAR (16102414; HKUST5/CRF/12R; AoE/M-09/12, and T13-607/12R), and the Innovation and Technology Commission of the HKSAR (ITCPD/17-9).

Supplementary data

Supplementary data to this article can be found online at https://doi.org/10.1016/j.jgg.2019.06.002.

References

Aachoui, Y., Sagulenko, V., Miao, E.A., Stacey, K.J., 2013. Inflammasome-mediated pyroptotic and apoptotic cell death, and defense against infection. Curr. Opin. Microbiol. 16, 319–326.
Barron, K.D., 1995. The microglial cell. A historical review. J. Neurol. Sci. 134 (Suppl. 1), 57–68.
Bergsbaken, T., Fink, S.L., Cookson, B.T., 2009. Pyroptosis: host cell death and inflammation. Nat. Rev. Microbiol. 7, 99–109.
Breitbach, K., Sun, G.W., Kohler, J., Eske, K., Wongprompitak, P., Tan, G., Liu, Y., Gan, Y.H., Steinmetz, I., 2009. Caspase-1 mediates resistance in murine melioidosis. Infect. Immun. 77, 1589–1595.
Chang, N., Sun, C., Gao, L., Zhu, D., Xu, X., Zhu, X., Xiong, J.W., Xi, J.J., 2013. Genome editing with RNA-guided Cas9 nuclease in zebrafish embryos. Cell Res. 23, 465–472.
Chen, G., Shaw, M.H., Kim, Y.G., Nunez, G., 2009. NOD-like receptors: role in innate immunity and inflammatory disease. Annu. Rev. Pathol. 4, 365–398.
Damm, A., Lautz, K., Kufer, T.A., 2013. Roles of NLRP10 in innate and adaptive immunity. Microb. Infect. 15, 516–523.
Danot, O., Marquenet, E., Vidal-Ingigliardi, D., Richet, E., 2009. Wheel of life, wheel of death: a mechanistic insight into signaling by STAND proteins. Structure 17, 172–182.
Davoust, N., Vuaillat, C., Androdias, G., Nataf, S., 2008. From bone marrow to microglia: barriers and avenues. Trends Immunol. 29, 227–234.
Diebolder, C.A., Halff, E.F., Koster, A.J., Huizinga, E.G., Koning, R.I., 2015. Cryoelectron tomography of the NAIP5/NLRC4 inflammasome: implications for NLR activation. Structure 23, 2349–2357.
Erzberger, J.P., Berger, J.M., 2006. Evolutionary relationships and structural mechanisms of AAA+ proteins. Annu. Rev. Biophys. Biomol. Struct. 35, 93–114.

Fernandes-Alnemri, T., Wu, J., Yu, J.W., Datta, P., Miller, B., Jankowski, W., Rosenberg, S., Zhang, J., Alnemri, E.S., 2007. The pyroptosome: a supramolecular assembly of ASC dimers mediating inflammatory cell death via caspase-1 activation. Cell Death Differ. 14, 1590–1604.
Fricker, M., Neher, J.J., Zhao, J.W., Thery, C., Tolkovsky, A.M., Brown, G.C., 2012. MFG-E8 mediates primary phagocytosis of viable neurons during neuro-inflammation. J. Neurosci. 32, 2657–2666.
Grimsley, C.M., Kinchen, J.M., Tosello-Trampont, A.C., Brugnera, E., Haney, L.B., Lu, M., Chen, Q., Klingele, D., Hengartner, M.O., Ravichandran, K.S., 2004. Dock180 and ELMO1 proteins cooperate to promote evolutionarily conserved Rac-dependent cell migration. J. Biol. Chem. 279, 6087–6097.
Gurung, P., Malireddi, R.K., Anand, P.K., Demon, D., Vande Walle, L., Liu, Z., Vogel, P., Lamkanfi, M., Kanneganti, T.D., 2012. Toll or interleukin-1 receptor (TIR) domain-containing adaptor inducing interferon-beta (TRIF)-mediated caspase-11 protease production integrates Toll-like receptor 4 (TLR4) protein- and Nlrp3 inflammasome-mediated host defense against enteropathogens. J. Biol. Chem. 287, 34474–34483.
Hall, C., Flores, M.V., Storm, T., Crosier, K., Crosier, P., 2007. The zebrafish lysozyme C promoter drives myeloid-specific expression in transgenic fish. BMC Dev. Biol. 7, 42.
Hanisch, U.K., Kettenmann, H., 2007. Microglia: active sensor and versatile effector cells in the normal and pathologic brain. Nat. Neurosci. 10, 1387–1394.
Herbomel, P., Thisse, B., Thisse, C., 2001. Zebrafish early macrophages colonize cephalic mesenchyme and developing brain, retina, and epidermis through a M-CSF receptor-dependent invasive process. Dev. Biol. 238, 274–288.
Hu, Z., Yan, C., Liu, P., Huang, Z., Ma, R., Zhang, C., Wang, R., Zhang, Y., Martinon, F., Miao, D., Deng, H., Wang, J., Chang, J., Chai, J., 2013. Crystal structure of NLRC4 reveals its autoinhibition mechanism. Science 341, 172–175.
Imamura, R., Wang, Y., Kinoshita, T., Suzuki, M., Noda, T., Sagara, J., Taniguchi, S., Okamoto, H., Suda, T., 2010. Anti-inflammatory activity of PYNOD and its mechanism in humans and mice. J. Immunol. 184, 5874–5884.
Jin, H., Li, L., Xu, J., Zhen, F., Zhu, L., Liu, P.P., Zhang, M., Zhang, W., Wen, Z., 2012. *Runx1* regulates embryonic myeloid fate choice in zebrafish through a negative feedback loop inhibiting *Pu.1* expression. Blood 119, 5239–5249.
Jin, H., Sood, R., Xu, J., Zhen, F., English, M.A., Liu, P.P., Wen, Z., 2009. Definitive hematopoietic stem/progenitor cells manifest distinct differentiation output in the zebrafish VDA and PBI. Development 136, 647–654.
Jorgensen, I., Miao, E.A., 2015. Pyroptotic cell death defends against intracellular pathogens. Immunol. Rev. 265, 130–142.
Kawai, T., Akira, S., 2009. The roles of TLRs, RLRs and NLRs in pathogen recognition. Int. Immunol. 21, 317–337.
Kayagaki, N., Stowe, I.B., Lee, B.L., O'Rourke, K., Anderson, K., Warming, S., Cuellar, T., Haley, B., Roose-Girma, M., Phung, Q.T., Liu, P.S., Lill, J.R., Li, H., Wu, J., Kummerfeld, S., Zhang, J., Lee, W.P., Snipas, S.J., Salvesen, G.S., Morris, L.X., Fitzgerald, L., Zhang, Y., Bertram, E.M., Goodnow, C.C., Dixit, V.M., 2015. Caspase-11 cleaves gasdermin D for non-canonical inflammasome signalling. Nature 526, 666–671.
Kayagaki, N., Warming, S., Lamkanfi, M., Vande Walle, L., Louie, S., Dong, J., Newton, K., Qu, Y., Liu, J., Heldens, S., Zhang, J., Lee, W.P., Roose-Girma, M., Dixit, V.M., 2011. Non-canonical inflammasome activation targets caspase-11. Nature 479, 117–121.
Kovacs, S.B., Miao, E.A., 2017. Gasdermins: effectors of pyroptosis. Trends Cell Biol. 27, 673–684.
Lamkanfi, M., Dixit, V.M., 2014. Mechanisms and functions of inflammasomes. Cell 157, 1013–1022.
Latz, E., Xiao, T.S., Stutz, A., 2013. Activation and regulation of the inflammasomes. Nat. Rev. Immunol. 13, 397–411.
Li, L., Jin, H., Xu, J., Shi, Y., Wen, Z., 2011. *Irf8* regulates macrophage *versus* neutrophil fate during zebrafish primitive myelopoiesis. Blood 117, 1359–1369.
Li, L., Yan, B., Shi, Y.Q., Zhang, W.Q., Wen, Z.L., 2012a. Live imaging reveals differing roles of macrophages and neutrophils during zebrafish tail fin regeneration. J. Biol. Chem. 287, 25353–25360.
Li, Y., Du, X.F., Liu, C.S., Wen, Z.L., Du, J.L., 2012b. Reciprocal regulation between resting microglial dynamics and neuronal activity *in vivo*. Dev. Cell 23, 1189–1202.
Man, S.M., Kanneganti, T.D., 2015. Gasdermin D: the long-awaited executioner of pyroptosis. Cell Res. 25, 1183–1184.
Miao, E.A., Rajan, J.V., Aderem, A., 2011. Caspase-1-induced pyroptotic cell death. Immunol. Rev. 243, 206–214.
Mullins, M.C., Hammerschmidt, M., Haffter, P., Nusslein-Volhard, C., 1994. Large-scale mutagenesis in the zebrafish: in search of genes controlling development in a vertebrate. Curr. Biol. 4, 189–202.
Nayak, D., Roth, T.L., McGavern, D.B., 2014. Microglia development and function. Annu. Rev. Immunol. 32, 367–402.
Park, D., Tosello-Trampont, A.C., Elliott, M.R., Lu, M., Haney, L.B., Ma, Z., Klibanov, A.L., Mandell, J.W., Ravichandran, K.S., 2007. Bai1 is an engulfment receptor for apoptotic cells upstream of the ELMO/Dock180/Rac module. Nature 450, 430–434.
Peri, F., Nusslein-Volhard, C., 2008. Live imaging of neuronal degradation by microglia reveals a role for v0-ATPase a1 in phagosomal fusion *in vivo*. Cell 133, 916–927.
Ran, F.A., Hsu, P.D., Wright, J., Agarwala, V., Scott, D.A., Zhang, F., 2013. Genome engineering using the CRISPR-Cas9 system. Nat. Protoc. 8, 2281–2308.
Shi, J., Zhao, Y., Wang, K., Shi, X., Wang, Y., Huang, H., Zhuang, Y., Cai, T., Wang, F., Shao, F., 2015. Cleavage of GSDMD by inflammatory caspases determines pyroptotic cell death. Nature 526, 660–665.
Shiau, C.E., Monk, K.R., Joo, W., Talbot, W.S., 2013. An anti-inflammatory NOD-like receptor is required for microglia development. Cell Rep. 5, 1342–1352.
Solnica-Krezel, L., Schier, A.F., Driever, W., 1994. Efficient recovery of ENU-induced mutations from the zebrafish germline. Genetics 136, 1401–1420.
Sun, G.W., Lu, J., Pervaiz, S., Cao, W.P., Gan, Y.H., 2005. Caspase-1 dependent macrophage death induced by Burkholderia pseudomallei. Cell Microbiol. 7, 1447–1458.
Svahn, A.J., Graeber, M.B., Ellett, F., Lieschke, G.J., Rinkwitz, S., Bennett, M.R., Becker, T.S., 2013. Development of ramified microglia from early macrophages in the zebrafish optic tectum. Dev. Neurobiol. 73, 60–71.
Trang, T., Beggs, S., Salter, M.W., 2011. Brain-derived neurotrophic factor from microglia: a molecular substrate for neuropathic pain. Neuron Glia Biol. 7, 99–108.
Wang, Y., Gao, W., Shi, X., Ding, J., Liu, W., He, H., Wang, K., Shao, F., 2017. Chemotherapy drugs induce pyroptosis through caspase-3 cleavage of a gasdermin. Nature 547, 99–103.
Wang, Y., Hasegawa, M., Imamura, R., Kinoshita, T., Kondo, C., Konaka, K., Suda, T., 2004. PYNOD, a novel Apaf-1/CED4-like protein is an inhibitor of ASC and caspase-1. Int. Immunol. 16, 777–786.
Watson, P.R., Gautier, A.V., Paulin, S.M., Bland, A.P., Jones, P.W., Wallis, T.S., 2000. Salmonella enterica serovars Typhimurium and Dublin can lyse macrophages by a mechanism distinct from apoptosis. Infect. Immun. 68, 3744–3747.
Westerfield, M., 1995. The Zebrafish Book: A Guide for the Laboratory Use of Zebrafish (*Danio rerio*), third ed. University of Oregon Press, Eugene, OR. 1995.
Xu, J., Wang, T., Wu, Y., Jin, W., Wen, Z., 2016. Microglia colonization of developing zebrafish midbrain is promoted by apoptotic neuron and lysophosphatidylcholine. Dev. Cell 38, 214–222.
Yan, B., Han, P., Pan, L., Lu, W., Xiong, J., Zhang, M., Zhang, W., Li, L., Wen, Z., 2014. IL-1beta and reactive oxygen species differentially regulate neutrophil directional migration and basal random motility in a zebrafish injury-induced inflammation model. J. Immunol. 192, 5998–6008.
Zakrzewska, A., Cui, C., Stockhammer, O.W., Benard, E.L., Spaink, H.P., Meijer, A.H., 2010. Macrophage-specific gene functions in Spi1-directed innate immunity. Blood 116, e1–e11.
Zhang, L., Chen, S., Ruan, J., Wu, J., Tong, A.B., Yin, Q., Li, Y., David, L., Lu, A., Wang, W.L., Marks, C., Ouyang, Q., Zhang, X., Mao, Y., Wu, H., 2015. Cryo-EM structure of the activated NAIP2-NLRC4 inflammasome reveals nucleated polymerization. Science 350, 404–409.
Zhen, F., Lan, Y., Yan, B., Zhang, W., Wen, Z., 2013. Hemogenic endothelium specification and hematopoietic stem cell maintenance employ distinct Scl isoforms. Development 140, 3977–3985.